Energy 258 (2022) 124665

Contents lists available at ScienceDirect

Energy

journal homepage: www.elsevier.com/locate/energy

A standing-wave, phase-change thermoacoustic engine: Experiments and model projections

Rui Yang [a,b], Avishai Meir [b], Guy Z. Ramon [b,c,*]

[a] Key Laboratory of Cryogenics, Technical Institute of Physics and Chemistry, Chinese Academy of Sciences, Beijing, 100190, China
[b] Department of Civil & Environmental Engineering, Technion – Israel Institute of Technology, Haifa, 32000, Israel
[c] The Nancy and Stephen Grand Technion Energy Program and Department of Civil & Environmental Engineering, Technion – Israel Institute of Technology, Haifa, 32000, Israel

ARTICLE INFO

Keywords:
Thermoacoustic engine
Wet thermoacoustics
Phase change
Wet stack
Low-grade heat recovery

ABSTRACT

Phase-change ('wet') thermoacoustic engines offer significant potential for efficient and clean conversion of low-grade heat. Previous work has demonstrated the effectiveness of phase-change in enhancing thermoacoustic conversion. However, this has thus far been limited to low mean pressure and low amplitude oscillations. In this work, we present a phase-change thermoacoustic engine able to work with high mean pressure and large amplitudes. In particular, we overcome issues related to liquid replenishment within the stack by using cellulose paper strips. The capillary action of the strips provides the means for rapid liquid absorption and circulation. Experimental results show that the temperature difference required to drive the engine is significantly decreased, to less than 90 °C, by phase change, while maintaining a pressure amplitude as high as 40 kPa under steady state. These results indicate that the offered design provides a promising pathway for advancing practical phase-change thermoacoustic devices. Furthermore, a theoretical investigation demonstrates the potential to reach a high efficiency (>40% of Carnot limit) when driven by low-grade heat sources at temperatures as low as 50 °C, provided that the heat transfer between the solid wall of heat exchangers and the fluid can be significantly improved, and the mass can be efficiently transported.

1. Introduction

A thermoacoustic engine is a type of heat engine, which converts heat into acoustic power or vice versa. Due to its minimal required moving parts, it exhibits advantages such as high reliability, low maintenance and potential low cost, while also being environmentally benign. Since the invention of the first thermoacoustic engine that demonstrated significant acoustic power generation [1], many efforts have been made to enhance the performance, mainly through improving the acoustic field for efficient thermoacoustic conversion and sound propagation [2]. To date, several prototypes have been reported reaching a performance similar to that of traditional engines [3–5]. Over the past decade, thermoacoustic engines with a looped configuration and multiple stages have been developed, showing great potential for low grade heat recovery [6–11]. However, the efficiency and the energy density of such systems are still lower than those of mature technologies, e.g., organic Rankine cycles and absorption refrigeration. On the other hand, the room for further improvement through traditional pathways, such as improving acoustics, is becoming increasingly small. This is most clearly seen in travelling–wave devices, where the achieved acoustic field is getting close to ideal.

One promising way to break through the bottleneck is to introduce pressure-induced mass transfer processes into the thermoacoustic conversion [12–14]. In the present work, a thermoacoustic engine incorporating mass transfer (phase change) is referred to as a 'wet' engine, in which a 'reactive' component that undergoes evaporation/condensation during oscillation is added into the classical working fluid (the 'inert' gas). In Fig. 1(a), we present the thermodynamic cycle of the conversion in a wet standing-wave thermoacoustic engine. Beginning from step (1), the mixture parcel moves towards the low-pressure (also low-temperature) region while being expanded adiabatically. Next, in step (2), the compression makes the vapor pressure higher than the local equilibrium, resulting in condensation, which is accompanied by the heat rejection to the wall. In steps (3) and (4), the reverse of steps (1) and (2), the parcel moves back towards the high-pressure (also high-temperature) region adiabatically, then absorbs heat from the solid

* Corresponding author. Department of Civil & Environmental Engineering, Technion – Israel Institute of Technology, Haifa, 32000, Israel.
E-mail address: ramong@technion.ac.il (G.Z. Ramon).

https://doi.org/10.1016/j.energy.2022.124665
Received 5 December 2021; Received in revised form 23 May 2022; Accepted 26 June 2022
Available online 15 July 2022
0360-5442/

wall, accompanied by the evaporation of the reactive component from the wall. Through this 4-step cycle, heat is converted into acoustic power. Compared with the classical thermoacoustic conversion, where only the inert component participates in the cycle, the addition of phase change can significantly enhance the conversion from the following two aspects: First, the periodic evaporation/condensation of the reactive component into/from the gas mixture can significantly increase the amplitude of volume and density oscillations, enhancing the acoustic oscillation; second, the addition of the time-averaged mass flux due to phase change can dramatically increase the enthalpy of the working fluid through the latent heat of phase change [14,15].

Recent studies have verified this concept to be an effective approach for improving the performance of thermoacoustic engines, particularly those driven by low-grade heat, as well as heat pumps. For example, a significant decrease (up to 200 °C) in the onset temperature has been observed by the addition of the phase change of water in both standing-wave and travelling-wave engines [12,16–18]. However, existing studies of phase-change thermoacoustic devices have mostly been limited to the onset process, or to the steady-state operation with low mean pressure (atmospheric pressure) and low amplitudes (within several kPa) [17,19–22].

Herein, we present a phase-change thermoacoustic engine that employs a novel stack made of cellulose strips, which enables the engine to operate steadily, in the wet mode, under a mean pressure of 10 bar, and at a large amplitude. Furthermore, a systematic numerical investigation was carried out, so as to probe the performance characteristics of the engine. The results illustrate that the improved design provides a promising pathway for advancing the performance of practical phase-change thermoacoustic devices.

2. Experimental setup

In a standing-wave system, thermoacoustic conversion occurs within a porous structure, called the 'stack' (as illustrated in Fig. 1(a), also referred to as a 'regenerator', in a travelling-wave system). The primary hindrance to the realization of high-amplitude, steady-state operation of a phase-change system is the material of the stack (or regenerator). First, the surface of the stack, where evaporation occurs (see Fig. 1(a)), must be replenished with liquid at a sufficient rate, otherwise it will dry out, halting the phase change. Second, the liquid condensed during the heat rejection step (see Fig. 1(a)) needs to be removed rapidly, or the channel of the stack may be blocked. Lastly, to efficiently complete the thermodynamic cycle, the hydraulic radius of the stack (half of the channel width in a parallel-plate structure) should be comparable to the thermal and diffusive penetration depths δ_α and δ_D ($\delta_\alpha \equiv (2\alpha/\omega)^{1/2}$ and $\delta_D \equiv (2D/\omega)^{1/2}$, where α and D are the thermal and molecular diffusivities, ω is the angular frequency [23]). The values of δ_α and δ_D are similar in the range of this study, especially when water and ammonia are used as reactive components (see supplementary material). Generally, the values of δ_α and δ_D decrease as the pressure is increased, since α and D decrease. Therefore, a smaller channel dimension is needed to keep the ratio of the hydraulic radius and the penetration depth when the mean pressure increases. To summarize, a proper stack should possess the following characteristics: strong capillary effect to transport liquid for steady evaporation, excellent absorbency for liquid and high hydrophilicity to avoid blockage, and small enough channel dimension. The most commonly-used material for the stack in wet engines is the cordierite ceramic honeycomb. However, it does not meet the above-mentioned requirements, and so faces the problems of liquid blockage and drying, and can only work for short times under low mean pressure [12,17–21,24,25].

Here, we present an improved design of the stack for wet engines, as illustrated in Fig. 1(b). It is made of approximately three hundred layers of cellulose paper strips (Whatman Grade 50), each 0.12 mm thick, with adjacent layers separated by 0.2 mm diameter copper wires. Note that the copper was chosen for its ease of acquisition and temperature resistance. Other materials with these advantages but a lower thermal conductivity may be better. As summarized in Table 1, we compare the absorbing-related characteristics of the stack made of cellulose paper with the traditional stack made of cordierite ceramics. The capillary action of the materials was estimated by soaking part of the material into water for 20 min, vertically, and then measuring the height of the wet section above the water. We found that the wet section of the cellulose strip was ~40 mm, while that of the cordierite was almost zero. It indicates that the cellulose can provide a strong driving force by significant capillary action for the returning flow of the liquid inside and along the solid walls of the stack. This flow transports the condensed liquid and the liquid stored in the low-temperature region towards the high-

Table 1
Comparison between the stacks made of cordierite ceramics and the cellulose paper. Absorbency, i.e., the ability to quickly absorb and store liquid, is specified by the ratio of water that the material can absorb over its own weight, and the time it takes to absorb it. r_h-hydraulic radius.

Material	Capillary action	Absorbency	Min. r_h
Cellulose	Strong	50%, <1 s	$\lesssim$ 0.1 mm
Cordierite	Very weak	25%, 15 min	~ 0.2 mm

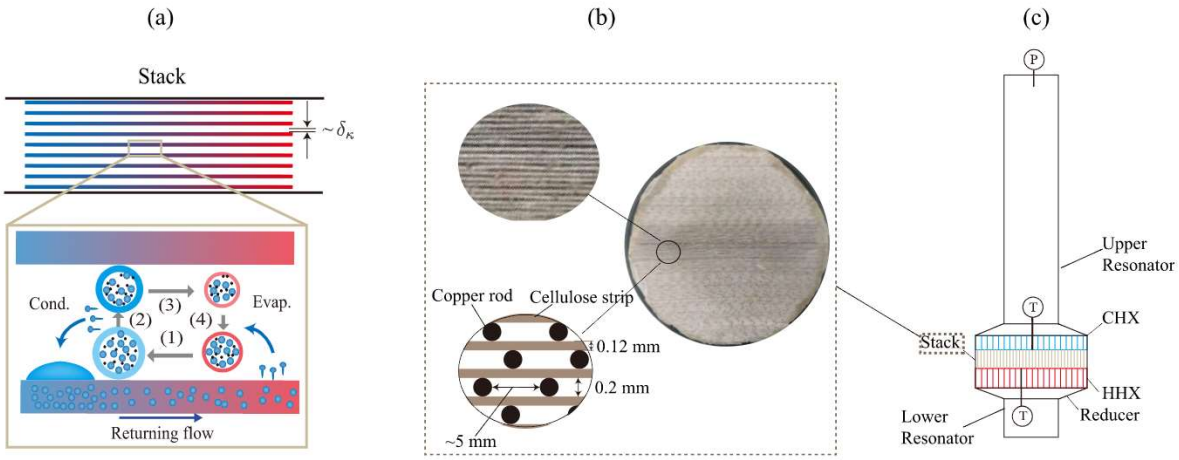

Fig. 1. (a) The thermodynamic cycle of the phase-change standing-wave thermoacoustic conversion: (1) adiabatic expansion, (2) isobaric heat rejection with mass loss, (3) adiabatic compression and (4) isobaric heat absorption with mass gain. (b) Structure of the stack. (c) Schematic of the phase-change standing-wave thermoacoustic engine. HHX-hot heat exchanger, CHX-cold heat exchanger. P-pressure sensor. T-thermocouple.

temperature region, and compensates for the mass loss due to evaporation. Furthermore, the absorbency of the two materials was also compared by measuring the weight of a piece of the material after the maximum amount of water was absorbed, while keeping the surface of the material without visible liquid film. We found that, the cellulose strip was able to absorb water equivalent to ~50% by weight within approximately 1 s, much faster than the cordierite, which could absorb water only ~25% of its weight. The excellent absorbency of the cellulose strip, and its highly hydrophilic prewetted surface, ensure that the condensed liquid is absorbed rapidly, preventing channel blockage. Additionally, the channel dimension of the cellulose stack can be controlled by adjusting the diameter of the wire spacer, allowing a hydraulic radius $\lesssim$0.1 mm, which is required by an engine operating under a high mean pressure.

To test the capacity of the cellulose and cordierite stacks to maintain a wet environment, we heated the stacks at a fixed HHX temperature of 220 °C, under atmospheric pressure and without the acoustic oscillations (see Fig. 2(a)). A temperature exceeding 100 °C in the stack was used as an indication of drying, since the presence of phase change fixes the temperature. As shown in Fig. 2(b), the cellulose stack can remain wet for at least 6 h (no sign of drying was observed at the end of the test), while the ceramic one becomes dry within 1 h. In conclusion, the presented stack provides a pseudo-constant liquid supply for the conversion, an essential feature for high amplitude operation.

With the cellulose stack as its 'core', a phase-change thermoacoustic engine, able to operate at a mean pressure of 10 bar for extended times, was constructed. The experimental system, shown in Fig. 1 (c), consists of a stack sandwiched between a cold heat exchanger (CHX) and a hot heat exchanger (HHX), within a cylindrical resonator. Both heat exchangers are made of copper. The HHX is the parallel-plate type, with two rows of three channels containing inserted cartridge heaters, enabling a total heating power of up to 1200 W. The CHX has a similar geometry, but with a wider gap between fins, in order to avoid blockage by condensed liquid. Some flax fiber was wound around the ends of each CHX fin, to remove the condensed liquid from the surface of the channel via capillary action. In this way, part of the condensed liquid could be delivered back onto the stack though the fiber, via gravity. Water, at constant temperature maintained by a chiller, was circulated through the CHX to absorb the rejected heat. Two reducers were used to connect the heat exchangers and the resonator. For detailed dimensions of each component, refer to Table 2.

A pressure sensor (GE UNIK 5000 series) was installed at the top of the resonator, and two K-type thermocouples were inserted into the heat exchangers. Their specific locations are shown by symbols 'P' and 'T' respectively in Fig. 1(c). In what follows, we define

Table 2
Dimensions of system components. HHX-hot heat exchanger, CHX-cold heat exchanger.

Item	lg. (mm)	dia. (mm)	r_h (mm)	Porosity
HHX	30	94	0.5	0.38
Stack	26	84	~ 0.1	~ 0.4
CHX	15	94	1.25	0.5
Upper resonator	890	47	23.5	1
Lower resonator	150	47	23.5	1
Reducer	100	–	–	1

$$\Delta T = T_h - T_c, \tag{1}$$

where T_h and T_c represent the temperatures measured by the two thermocouples in the HHX and the CHX respectively. Meanwhile, we also define the effective temperature difference as

$$\Delta T_g = T_{h,g} - T_{c,g}, \tag{2}$$

where $T_{h,g}$ and $T_{c,g}$ are the temperatures of the working fluid at the hot and cold ends of the stack.

In the experiments, nitrogen was used as the inert gas, while water and ethanol were used as the reactive component . In the wet-mode experiments (i.e., with phase change), 50 g of liquid, which is approximately half of the weight of the dry stack itself, was uniformly sprayed on the surface of the stack 30 minutes before each experiment. The flax fiber on the CHX also required prewetting, achieved by spraying some liquid. We note that the channels of the stack became distorted after repeated wetting and drying —some became wider and some narrower, due to some swelling of the material (see supplementary material). The widened channels were narrowed again by inserting pieces of the cellulose. In the dry-mode experiments (i.e., without phase change), the stack was dried in an oven at 140 °C for 4 h, to ensure no liquid was left in the stack.

3. Theoretical model

The phase-change thermoacoustic conversion process can be described by a linear theory, which was first developed by Raspet et al. [12] and Slaton et al. [13]. This theory was recently expanded by Weltsch et al. [15] and Offner et al. [14] to describe the thermoacoustic conversion incorporated with mass exchange processes, including condensation/evaporation but also extendable to reversible reactions such

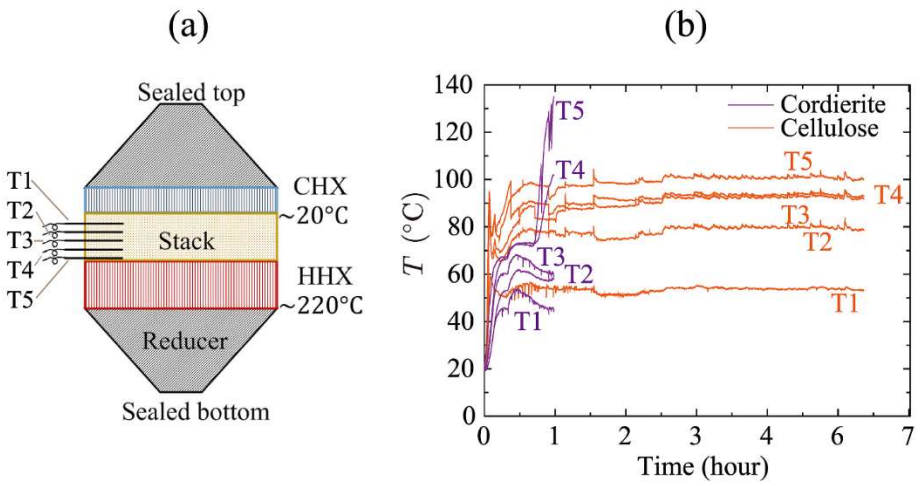

Fig. 2. (a) Schematic of the engine core for testing the abilities of the cellulose and cordierite stacks to maintain a wet environment. HHX-hot heat exchanger. CHX-cold heat exchanger. T1 to T5 represent five thermocouples. The solid temperature of the hot heat exchanger was kept at 220 °C, and the CHX was cooled by water at 20 °C. (b) Temperature profiles of the cellulose stack and the cordierite ceramic stack.

as absorption or adsorption. Herein, the equations presented in Offner et al. [14] (dimensional form) were used to model the phase-change thermoacoustic engine. These are given by

$$\frac{dp_1}{dx} = -\frac{i\omega\rho_m}{F_\nu A_g} U_1, \tag{3}$$

$$\frac{dU_1}{dx} = -\frac{i\omega A_g}{\rho_m a^2}\left[\gamma + F_\alpha(1-\gamma) + \gamma\frac{C_\mathrm{m}}{1-C_\mathrm{m}}\frac{1-F_D}{\eta_\mathrm{D}}\right]p_1 + \left[\frac{F_\nu - F_\alpha}{(1-Pr)F_\nu}\beta + \frac{\frac{\eta_\nu}{\eta_\mathrm{D}}(1-F_D)-(1-F_\nu)}{F_\nu(1-Sc)}\frac{C_\mathrm{m}}{1-C_\mathrm{m}}\frac{l_\mathrm{h}}{R_\mathrm{g}T_\mathrm{m}^2}\right]\frac{dT_m}{dx}U_1, \tag{4}$$

$$\frac{dT_m}{dx} = \frac{\dot{H}_2 - \frac{1}{2}\Re\left[p_1\widetilde{U}_1\left(1-\frac{\widetilde{F}_\nu - F_g}{(1+Pr)F_\nu}\right)\right] - \dot{m}l_\mathrm{h}}{\frac{\rho_m c_p|U_1|^2}{2A_g\omega(1-Pr)|F_\nu|^2}\Im\left[\frac{\widetilde{F}_\nu - F_\alpha}{1+Pr} - \widetilde{F}_\nu\right] - \left(A_g k + A_s k_s\right)}. \tag{5}$$

In these equations, p_1 and U_1 are the pressure amplitude and the volumetric velocity amplitude, respectively. T_m, ρ_m, a, c_p, γ, β, Pr and Sc denote the mean temperature, the density, the speed of sound, the heat capacity, the specific heat ratio, the thermal expansion coefficient, the Prandtl number and the Schmidt number of the mixture, respectively. R_g is the universal gas constant with the value of 8.314 J/K·mol, ω is the angular frequency, k and k_s represent the thermal conductivity of the gas and solid, respectively, l_h is the latent heat of the reactive component and A_g and A_s represent the cross-sectional area for gas and solid, respectively. η_ν and η_D reflect the effects from sorption kinetics, and are assumed to be unity in the gas-liquid phase change [14]. The symbols $\Re$ and $\Im$ denote the real and imaginary parts of a complex number. In addition, the variation of the total energy flux is governed by

$$\frac{d\dot{H}_2}{dx} = \dot{q} \tag{6}$$

in which $\dot{H}_2$ is the total energy flux and $\dot{q}$, the change rate of $\dot{H}_2$ along the axial direction, is assumed to be zero in all components except within the heat exchangers. In equation (5), $\dot{m}$ is the time-averaged mass flux of the reactive component in the axial direction due to the periodical phase change, and is calculated via [15]

$$\dot{m} = \frac{1}{1-C_\mathrm{m}}\frac{C_\mathrm{m}}{2R_\mathrm{g}T_\mathrm{m}}\Re\left[p_1\widetilde{U}_1\frac{F_\mathrm{D}-\widetilde{F}_\nu}{(1+Sc)\widetilde{F}_\nu}\right] - \frac{1}{1-C_\mathrm{m}}\frac{|U_1|^2}{2A_g\omega|F_\nu|^2}\frac{p_\mathrm{m}C_\mathrm{m}l_\mathrm{h}}{R_g^2T_\mathrm{m}^3}\frac{1}{1-Sc^2}\Im\left[\widetilde{F}_\nu(1+Sc) + \frac{\eta_\nu}{\eta_\mathrm{D}}\left(F_\mathrm{D}-\widetilde{F}_\nu\right)\right]\frac{dT_\mathrm{m}}{dx} - \frac{p_\mathrm{m}A_g D}{1-C_\mathrm{m}}\frac{C_\mathrm{m}l_\mathrm{h}}{R_\mathrm{g}^2T_\mathrm{m}^3}\frac{dT_\mathrm{m}}{dx}. \tag{7}$$

For steady-state operation, $\dot{m}$ must equal the amount of liquid pumped through the capillary action [13,14]. C_m, the mean concentration of the reactive component, is determined by the local pressure, temperature and the properties of the reactive component, which is subjected to the Clausius-Clapeyron relation

$$C_m = \exp\left[-\frac{l_h}{R_g}\left(\frac{1}{T_m}-\frac{1}{T_b}\right)\right], \tag{8}$$

where T_b is the boiling temperature of the reactive species. Finally, the functions F_n ($n = \alpha$, ν, or D) describe the spatial-average effect arising from the velocity, pressure, temperature and concentration fields. In a stack with a geometry of parallel channels, as used in this work, F_n can be calculated through

$$F_n = 1 - \frac{\tanh\left[(1+\mathrm{i})\tau_n/\sqrt{2}\right]}{(1+\mathrm{i})\tau_n/\sqrt{2}} \tag{9}$$

where $\tau_n \equiv r_h\sqrt{\omega/n}$ is the Womersley number, in which r_h is the hydraulic radius.

The ODEs (Eqs. (3) to (6)) are integrated along the axis direction, starting from the top of the engine, through a forth-order Runge-Kutta method. However, there are two unknown parameters at the beginning of the integration, which are the frequency and the pressure amplitude. To closed the problem, a shooting method is utilized, whereby two target values are used, namely $\Im[U_1] = 0$ and $\Re[U_1] = 0$ at the bottom of the system, due to the closed boundary. Then the unknown parameters can be solved. Consequently, the frequency, and the distributions of p_1, U_1, T_m and C_m in the system can be obtained. The acoustic power can be calculated through $\dot{E}_2 = \frac{1}{2}\Re[\widetilde{p}_1 U_1]$.

Additionally, a source term arises upon rearranging Eq. (4), which can be expressed as (see supplementary material for full derivation)

$$g \approx g_{dry}\left(1 + \frac{C_m}{1-C_m}\frac{l_h}{R_g T_m}\right). \tag{10}$$

In Eq. (10), g_{dry} is the source term in the classical thermoacoustic conversion, given by

$$g_{dry} = \frac{F_\nu - F_\alpha}{(1-Pr)F_\nu}\frac{1}{T_m}\frac{dT_m}{dx}. \tag{11}$$

In thermoacoustic theory, this term is the only one that directly contributes to the thermoacoustic conversion [23,26]. In the following discussion, it will be used for analyzing the performance of the system.

4. Results and discussion

4.1. Experimental performance

We first discuss the experimental results. Fig. 3(a) and (b) show the dependence of the pressure amplitude, $|p_1|$, and the hot-end temperature T_h, on the temperature difference ΔT, in both dry and wet cases (in which ethanol or water serves as the reactive component). By comparing the curves of the wet and dry modes, it is clear that the presence of phase change can significantly decrease the temperature difference required to achieve a given pressure amplitude. For example, when the mean pressure is 10 bar, in order to achieve $|p_1| \sim 20$ kPa, the dry-mode engine requires $\Delta T > 120$ °C, while the wet-mode engine operates at $\Delta T \sim 60$ °C and ~ 70°C when ethanol and water are used as the reactive component, respectively.

Further, for a fixed ΔT, $|p_1|$ with ethanol as the reactive component is higher than that with water when $\Delta T < 70$ °C, because the boiling temperature of ethanol is lower than that of water, leading to a higher concentration C_m. However, when ΔT is increased beyond 70 °C, using water results in a larger $|p_1|$, possibly because C_m becomes too high for ethanol at the high values of T_h, at which point the rate of evaporation exceeds the ability of the stack to supply liquid at a sufficient rate. Consequently, part of the stack becomes dry, which limits the phase-change thermoacoustic conversion. Additionally, in classical thermoacoustic engines, the increase of mean pressure at a given temperature difference generally amplifies the oscillation [27]. However, this is not necessarily so for wet thermoacoustic engines. For example, when the temperature difference is ~ 50°C, increasing the mean pressure from 7.5 bar to 10 bar slightly decreases the pressure amplitude. This is because the boiling temperature of the reactive component is increased, leading to a decrease in C_m (see Eq. (8)), thereby weakening the phase-change thermoacoustic conversion.

To further investigate the influence of the reactive component concentration on the conversion, in Fig. 3 (c) we show the pressure amplitude $|p_1|$ with different hot-end temperature T_h, while keeping the temperature difference ΔT fixed. Two groups of results are shown, one with ethanol as the reactive component and $\Delta T = 56$ °C, while the other one is with water and $\Delta T = 67$ °C. In both curves, a higher T_h (indicating

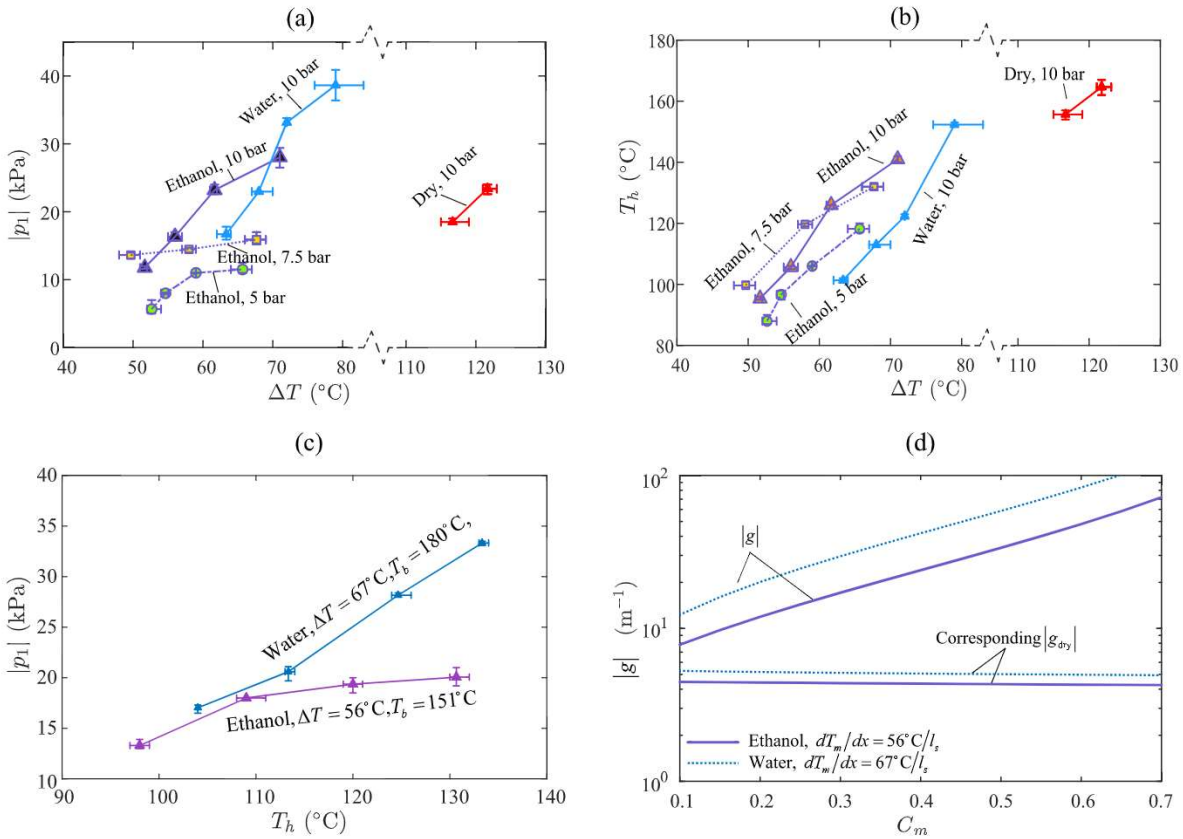

Fig. 3. Experimental results: (a) The relation between $|p_1|$, the pressure amplitude at the closed-end of the resonator, and the temperature difference across the stack, ΔT. (b) The relation between the temperature at the hot end and the temperature difference. (c) The relation between the pressure amplitude at the closed-end of the resonator and the temperature at the hot end. The mean pressure is 10 bar. (d) The magnitudes of the source term $|g|$ (see Eqs. (10) and (11)) under different values of C_m. Note that $|g_{dry}|$ is independent of C_m (see Eq. (11)). Therefore, the horizontal axis, i.e., C_m, actually denotes the corresponding temperature for $|g_{dry}|$ according to Eq. (8).

a larger C_m) helps amplify the oscillation at a fixed ΔT. The main reason for this is the enhanced source term (see Eq. (10)) with the increased temperature, which is a result of the increase of the reactive component's concentration C_m.

In Fig. 3(d), the values of $|g|$ are shown to increase steadily as C_m (or T_m) is increased, which is in accordance with Eq. (10). This feature is unique to the wet thermoacoustic engine. In contrast, for classical thermoacoustic engines, increasing the ambient temperature always leads to a reduced performance [28], manifested by either an increased temperature difference or a reduced pressure oscillation, because the kinematic viscosity of the gas increases with the temperature. This is also reflected in Fig. 3(d), where $|g_{dry}|$ decreases gradually and slightly as T_m is increased (or C_m, see Eq. (8)). Additionally, $|g|$ is higher for water than for ethanol, due to the larger temperature gradient imposed, and the higher latent heat of water.

According to Eq. (10), the thermoacoustic conversion can always be enhanced by increasing the temperature towards the boiling temperature (i.e., $C_m \to 1$). However, the curve for ethanol becomes flat when $T_h > 110$ °C, indicating that the enhancement due to phase change becomes less significant, possibly due to partial drying of the stack. In general, the time-averaged mass flux due to evaporation can be represented by $\dot{m}$, which is proportional to $C_m/(1 - C_m)$ [14], indicating a more significant flux under a higher C_m. During the operation, part of the mass evaporated from the stack condensed on the wall of the stack, and then was transported back via capillary action, to compensate for the evaporation. However, some of the evaporated mass condensed on the wall of the resonator outside the stack area, and so was lost from the cycle. Therefore, the stack will eventually dry out when all the liquid stored in it escapes, unless the liquid is recovered and returned to the hot side of the stack. At small values of C_m, this process took several hours, enough for prolonged steady-state experiments; however, when C_m was large, part of the stack became dry before the steady-state was reached, weakening the positive effect of phase change.

4.2. Model-based performance projection

As shown in Fig. 4, the calculated results from the model show reasonable quantitative agreement with the experimental data, providing a solid foundation for the following theoretical analysis. The calculated values of $|p_1|$ are higher than the corresponding experimental data, mainly attributed to the distortion of the channels of the stack (see supplementary material), which is not included in the model.

Next, we explore the performance of the engine based on the model. Since the stack is the only component producing acoustic power, we define the efficiency of the engine as

$$\eta = E_s/Q_{in}, \tag{12}$$

where E_s is the acoustic power generated in the stack, and Q_{in} is the input heat. As can be seen in Fig. 5(a), the efficiency, η, drops with the increase of T_h, despite the increased pressure amplitude ,$|p_1|$. The reason behind this is that the effective temperature difference ΔT_g (definition see Eq. (2)) is reduced due to the increase of the temperature difference for heat transfer, although ΔT is fixed. We note that the values of η are relatively low, which is mainly ascribed to the low acoustic impedance $|z|$ (defined as $|p_1|/|v_1|$, where $|v_1|$ is the velocity amplitude) in the stack, which is approximately $\rho_m a$, indicating that viscous losses are severe. However, the acoustic impedance can be increased by locally enlarging the cross-sectional area of the stack. In Fig. 5(b), we present the relation between

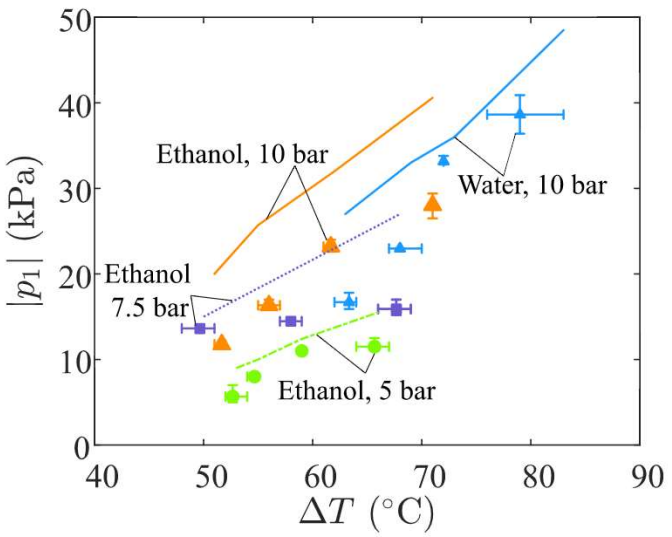

Fig. 4. Comparison between the experimental and calculated results. The dots and curves represent the experimental and the corresponding calculated results, respectively.

the efficiency η and the area ratio $A_{g,s}/A_r$, where A_r is the cross-sectional area of the resonator, $A_{g,s} = A_s\varphi_s$ is the gas area of the stack, with A_s and φ_s being the cross-sectional area and the porosity of the stack. As may be seen, the average acoustic impedance $|z|_m$ of the stack can be effectively increased by enlarging $A_{g,s}/A_r$, leading to an increased η, until reaching a peak value of 2.3% when $A_{g,s}/A_r = 8$. This efficiency corresponds to 19% of Carnot limit, if we ignore the temperature differences for heat transfer and use gas temperatures $T_{h,g}$ and $T_{c,g}$ to calculate the Carnot efficiency. In the experimental setup, $A_{g,s}/A_r = 1.3$, only about half of the initial design value, because many of the channels were blocked by the glue used for fixing the cellulose strips. Additionally, some extra cellulose strips were inserted into the stack to fill the gaps enlarged due to the distortion after use, which also reduced $A_{g,s}$. Furthermore, another important factor determining the thermoacoustic conversion process is the Womersley number, τ_ν, which represents the ratio of the oscillation time scale to the viscous time scale [29]. In Fig. 5(c), we can see that the optimal values of τ_ν for highest efficiencies are around 3 for all curves. A smaller τ_ν leads to severe viscous loss, and a larger τ_ν indicates insufficient use of the channel cross-section, leading to lower efficiencies. The value of τ_ν in the experiments is ~ 2.5, near the optimal value.

As revealed in Yang et al. [17,19], the temperature range of a phase-change thermoacoustic system should be near the boiling temperature of the reactive species, to take full advantage of phase change. Due to the relatively high boiling temperatures of water and ethanol (180 °C and 151 °C under 10 bar respectively), values of T_h were often above 100° in the experiments, limiting the heat sources it could utilize, although the temperature difference required to drive the engine was small. To relieve this issue, in Fig. 6, we explore the performance of the engine with ammonia as the reactive component, whose boiling temperature is 74 °C under the mean pressure of 40 bar. As can be seen in Fig. 6(a), both the effective temperature difference ΔT_g and the concentration of the reactive species at the hot end $C_{m,h}$, increase with the rise of the input heat Q_{in}. Since the cold-end temperature of the fluid, $T_{c,g}$ is fixed at 25 °C, the engine has the potential to utilize heat sources at temperatures as low as 50 °C (ignoring the temperature difference for heat transfer in heat exchangers). Furthermore, as shown in Fig. 6(b), a relatively high efficiency, namely 30%–40% of the Carnot limit, can be obtained, with the generated acoustic power E_s up to 100 W.

This projected performance is encouraging. However, there are two issues that might hinder the development of such an efficient system. The first one is the heat transfer between the heat exchanger and the working fluid, for which the required temperature difference may be considerable. For instance, the required temperature differences with the current HHX are 20 °C and 78 °C when Q_{in} are 10^3 W and 10^4 W, respectively. Therefore, the heat transfer between solid and gas in the heat exchanger must be significantly improved, otherwise the advantage of low-grade heat recovery will be significantly reduced. Limited by the finite thermal penetration depth and the velocity amplitude in the oscillatory flow, this heat transfer can be hardly lifted when traditional heat exchangers are used. Potential methods include using the phase change to help transfer heat, and utilizing the acoustic self-pumped steady flow [30]. The second issue is the liquid replenishment required to overcome the effect of the time-averaged mass flux of the reactive species. This mass flux is the time-averaged effect of the periodic evaporation and condensation during the oscillation, therefore it requires the solid wall of the stack to absorb a large amount of liquid instantaneously and to transport the liquid to the region where evaporation occurs , otherwise the channel will be blocked and the phase change will halt. The mass flux increases with the rise of Q_{in} — from 0.7 g/s to 8.8 g/s when Q_{in} is increased from 10^3 W to 10^4 W. This poses significant challenges for the material and structure of the stack.

5. Conclusions

To summarize, we present a phase-change thermoacoustic engine able to work at a high mean pressure and a large amplitude. A stack made of cellulose paper strips was designed to ensure sufficient liquid supply and rapid liquid absorption during the phase-change thermoacoustic conversion. Experimental results demonstrate a significant reduction of the temperature difference required to drive the engine and a pressure amplitude as high as 40 kPa, which is one order of magnitude higher than previously reported. The stack may become partly dry with a large concentration of the reactive component, leading to deterioration in performance. This problem is likely to be solved by adding a liquid source near the stack, so that the liquid can be supplied through

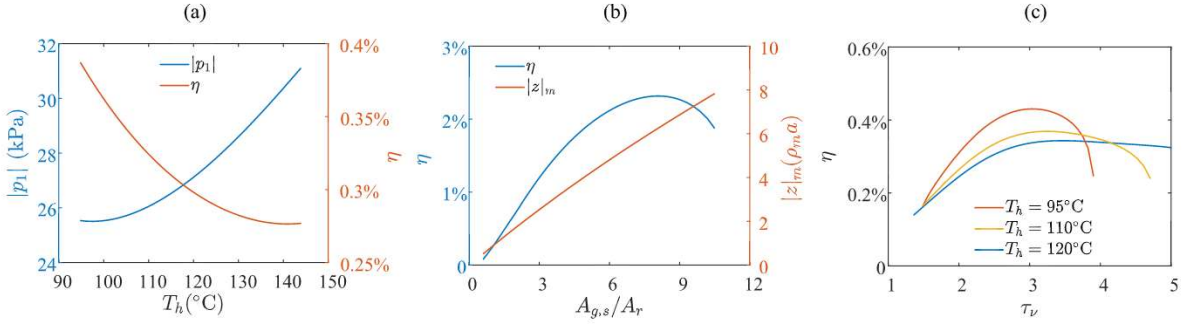

Fig. 5. Calculated results: (a) The pressure amplitude $|p_1|$ and the efficiency η vs. the hot temperature T_h. (b) The influence of the area ratio $A_{g,s}/A_r$ on the efficiency η and the mean acoustic impedance $|z|_m$. (c) The influence of the Womersley number τ_ν on the efficiency η. The working mixture is nitrogen and ethanol, the mean pressure is 10 bar $\Delta T = 56$ °C.

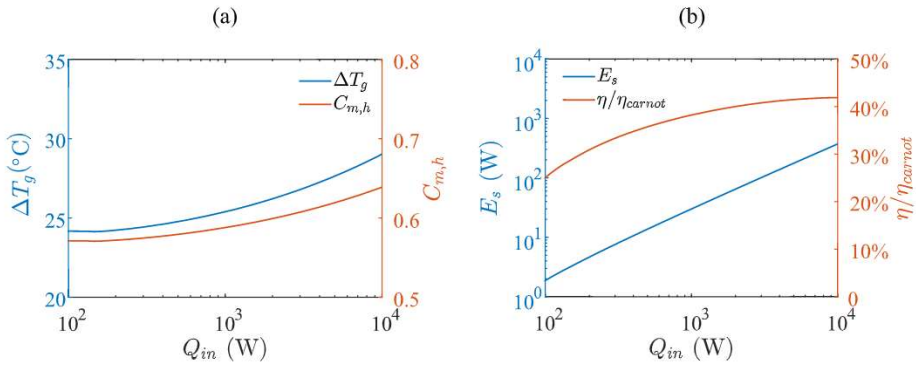

Fig. 6. Projected performance of the engine with ammonia as the reactive species and 40 bar mean pressure, with different input heat Q_{in}: (a) Temperature difference of the working fluid ΔT_g and the concentration of the reactive species at the hot end $Cm,_h$. (b) Acoustic power generated in the stack E_s and the relative Carnot efficiency η/η_{carnot}. The Carnot efficiency η_{carnot} is defined with the gas temperatures $T_{h,g}$ and $T_{c,g}$. The temperature of the working fluid at the cold end is 25 °C. $A_{g,s}/A_r = 8$. $\tau_\nu = 3$.

strong capillary action. Further theoretical analysis demonstrated the potential to operate as an effective engine f or recovering low-grade heat at temperatures as low as 50 °C. The proposed design, especially that of the stack, paves the way for practical phase-change thermoacoustic devices.

Credit author statement

Rui Yang: Conceptualization, Methodology, Software, Data curation, Validation, Investigation, Writing – original draft, Project administration. **Avishai Meir:** Resources, Methodology, Data curation, Writing – original draft. **Guy Z. Ramon:** Conceptualization, Writing – review & editing, Project administration, Funding acquisition.

Declaration of competing interest

The authors declare that they have no known competing financial interests or personal relationships that could have appeared to influence the work reported in this paper.

Acknowledgments

The research was supported by grant 219-11-127 from the Israel Ministry of Energy and Water. R.Y. was supported, in part, by a fellowship from the Israel Council for Higher Education.

Appendix A. Supplementary data

Supplementary data to this article can be found online at https://doi.org/10.1016/j.energy.2022.124665.

References

[1] Feldman KT, Carter RL. A study of heat driven pressure oscillations in a gas. J Heat Tran 1970;92(3):536–40.
[2] Chen G, Tang L, Mace B, Yu Z. Multi-physics coupling in thermoacoustic devices: a review. Renew Sustain Energy Rev 2021;146:111170.
[3] Backhaus S, Swift GW. A thermoacoustic stirling heat engine. Nature 1999;399 (6734):335.
[4] Bi T, Wu Z, Zhang L, Yu G, Luo E, Dai W. Development of a 5 kW traveling-wave thermoacoustic electric generator. Appl Energy 2017;185:1355–61.
[5] Jin T, Huang J, Feng Y, Yang R, Tang K, Radebaugh R. Thermoacoustic prime movers and refrigerators: thermally powered engines without moving components. Energy 2015;93:828–53.
[6] Yang R, Wang Y, Jin T, Feng Y, Tang K. Development of a three-stage looped thermoacoustic electric generator capable of utilizing heat source below 120 C. Energy Convers Manag 2018;155:161–8.
[7] de Blok K. Multi-stage traveling wave thermoacoustics in practice. In: 19th international congress sound vibration. Vilnius: Citeseer; 2012.
[8] Xu J, Luo E, Hochgreb S. Study on a heat-driven thermoacoustic refrigerator for low-grade heat recovery. Appl Energy 2020;271:115167.
[9] Xu J, Luo E, Hochgreb S. A thermoacoustic combined cooling, heating, and power (CCHP) system for waste heat and LNG cold energy recovery. Energy 2021;227: 120341.
[10] Abdoulla-Latiwish KO, Jaworski AJ. Two-stage travelling-wave thermoacoustic electricity generator for rural areas of developing countries. Appl Acoust 2019;151: 87–98.
[11] Al-Kayiem A, Yu Z. Using a side-branched volume to tune the acoustic field in a looped-tube travelling-wave thermoacoustic engine with a RC load. Energy Convers Manag 2017;150:814–21.
[12] Raspet R, Slaton WV, Hickey CJ, Hiller RA. Theory of inert gas-condensing vapor thermoacoustics: propagation equation. J Acoust Soc Am 2002;112(4):1414–22. https://doi.org/10.1121/1.1508113. ISSN 0001-4966.
[13] Slaton WV, Raspet R, Hickey CJ, Hiller RA. Theory of inert gas-condensing vapor thermoacoustics: transport equations. J Acoust Soc Am 2002;112(4):1423–30. https://doi.org/10.1121/1.1508114. ISSN 0001-4966.
[14] Offner A, Yang R, Felman D, Elkayam N, Agnon Y, Ramon GZ. Acoustic oscillations driven by boundary mass exchange. J Fluid Mech 2019;866:316–49. https://doi.org/10.1017/jfm.2019.87. ISSN 0022-1120, 1469-7645.
[15] O. Weltsch, A. Offner, D. Liberzon, G. Z. Ramon, Adsorption-mediated mass streaming in a standing acoustic wave, Phys Rev Lett 118 (24), ISSN 0031-9007, 1079-7114, doi:10.1103/PhysRevLett.118.244301.
[16] Meir A, Offner A, Ramon GZ. Low-temperature energy conversion using a phase-change acoustic heat engine. Appl Energy 2018;231:372–9. https://doi.org/10.1016/j.apenergy.2018.09.124. ISSN 03062619.
[17] Yang R, Meir A, Ramon GZ. Theoretical performance characteristics of a travelling-wave phase-change thermoacoustic engine for low-grade heat recovery. Appl Energy 2020;261:114377.
[18] Tsuda K, Ueda Y. Critical temperature of traveling- and standing-wave thermoacoustic engines using a wet regenerator. Appl Energy 2017;196:62–7. https://doi.org/10.1016/j.apenergy.2017.04.004. ISSN 03062619.
[19] Yang R, Blanc N, Ramon GZ. Environmentally-sound: an acoustic-driven heat pump based on phase change. Energy Convers Manag 2021;232:113848.
[20] Blayer Y, Elkayam N, Ramon GZ. Phase-dependence of sorption-induced mass streaming in an acoustic field. Appl Phys Lett 2019;115(3):033703. https://doi.org/10.1063/1.5110601. ISSN 0003-6951, 1077-3118.
[21] Senga M, Hasegawa S. Energy conversion of thermoacoustic engines with evaporation and condensation. Int J Heat Mass Tran 2021;165:120385.
[22] Brustin T, Offner A, Ramon GZ. Effect of gas mixture on temperature and mass streaming in a phase-change thermoacoustic engine. Appl Phys Lett 2020;116(24): 243701. https://doi.org/10.1063/5.0009599. ISSN 0003-6951, 1077-3118.
[23] Swift GW. Thermoacoustics: a unifying perspective for some engines and refrigerators. ASA; 2003.
[24] Noda D, Ueda Y. A thermoacoustic oscillator powered by vaporized water and ethanol. Am J Phys 2013;81(2):124–6.
[25] Tsuda K, Ueda Y. Abrupt reduction of the critical temperature difference of a thermoacoustic engine by adding water. AIP Adv 2015;5(9):097173.
[26] Rott N. Thermoacoustics. Adv Appl Mech 1980;20:135–75.
[27] T. Jin, R. Yang, Y. Wang, Y. Feng, K. Tang, Low temperature difference thermoacoustic prime mover with asymmetric multi-stage loop configuration, Sci Rep 7.
[28] Qiu L, Lou P, Wang K, Wang B, Sun D, Rao J, Zhang X. Characteristics of onset and damping in a standing-wave thermoacoustic engine driven by liquid nitrogen. Chin Sci Bull 2013;58(11):1325–30.
[29] Yazaki T, Iwata A, Maekawa T, Tominaga A. Traveling wave thermoacoustic engine in a looped tube. Phys Rev Lett 1998;81(15):3128.
[30] Swift G, Backhaus S. A resonant, self-pumped, circulating thermoacoustic heat exchanger. J Acoust Soc Am 2004;116(5):2923–38.